Caliphate Journal of Science & Technology (CaJoST)

ISSN: 2705-313X (PRINT); 2705-3121 (ONLINE) Research Article

Open Access Journal available at: https://cajost.com.ng/index.php/files and https://www.ajol.info/index.php/cajost/index

DOI: https://dx.doi.org/10.4314/cajost.v6i2.11

Article Info

Received: 29th April 2024

Revised: 10th June 2024

Accepted: 14th June 2024

[1]Department of Chemical and Geological Sciences; Al-Hikmah University; Ilorin; Nigeria
[2]Department of Chemistry; Faculty of Physical Sciences; University; Ilorin; Nigeria.
[3]Department of Pure and Applied Chemistry; Osun State University; Osogbo ; Nigeria

***Corresponding author's email:**

lakunleayinla@gmail.com

Cite this: *CaJoST*, 2024, 2, 217-229

Synthesis and Biological Activity of Mixed Ligand Metal Complexes of 6-Mercaptopurine - Nicotinamide

[1]Sheriff O. Ayinla, [2]Abdullah O. Rajee, [2]Kamil O. Yusuff., [2]Ginikachukwu G. Mbaeyi, [2;3]Hassan K. Busari and [2]Joshua A. Obaleye

Biological activity of a ligand improves when it is coordinated with a metal ion. Mixed ligand metal complexes of 6-mercaptopurine and nicotinamide were synthesized using one-pot synthetic methods. Spectroscopic methods were used to characterize the mixed ligand metal complexes. The spectroscopic analysis of the complexes supports the formation of the compounds in which the exocyclic sulphur (S-6) atom on the pyrimidine ring of the 6-mercaptopurine and its N(7) atom of the imidazole ring allow the ligand to act as bidentate while the nicotinamide coordinates as a monodentate ligand only through the nitrogen atom of its pyridinic ring. Thermogravimetric analysis of the compounds is in agreement with the proposed structures. Evaluation of the thermodynamic activated parameters of the complexes shows high positive values for the ΔG and negative values for the entropy of activation, which is an indication that the decomposition of the complexes is non-spontaneous and the compounds have a more ordered structure compared to the ligands. The DFT studies revealed low LUMO–HOMO energy gap (ΔE) values of 3.255 eV and 1.029 eV for the compounds **(1)** [Zn(mp)(nic)EtOH] and **(2)** [Ni(mp)(nic)(Ac)].4H_2O respectively, in ethanol medium. Compound **(1)** is a better antioxidant agent compared to compound **(2)** but compound **(2)** shows improved antimicrobial activity compare to compound **(1)**. Experimental results show improved antioxidant activity for the [Zn(mp)(nic)EtOH] complex, which correlates with the findings from the docking experiment and the complex docked alongside allopurinol at binding pocket I with a binding affinity value of –6.4 kcal mol^{-1}, showing its antioxidant potential.

Keywords: 6-mercaptopurine, nicotinamide, thermodynamics activated parameters, density functional theory.

1. Introduction

An analogue of the natural purine hypoxanthine is 6-Mercaptopurine ($C_5H_4N_4S$), which is an important antitumor drug for treating human leukemia. The study of the synthesis of 6-mercaptopurine metal complexes has shown the ligand to coordinate through atoms of the S(6) and N(7) of the pyrimidine ring but preferentially bind through the S(6) atom serving as monodentate ligand.[1,2] Nicotinamide coordinates only through the N-atom of its pyridinic ring, therefore regarded as a monodentate ligand when the structure of the mixed ligand of amoxicillin and 4-chlorobenzophenone metal complexes was elucidated.[3] It behaves as an ambidentate ligand, coordinating through the nitrogen of the pyridinic ring as well as the oxygen atom of the carbonyl group in the synthesis of the nicotinamide and 2,2'-bipyridine mixed ligand metal complexes.[4]
Trace elements are required in small quantities by the body system and are said to be essential to the optimal healthy maintenance of the system. Such elements are iron, copper, chromium, zinc etc. The metals, either in ionic form or molecule, are absorbed by the human body by developing homeostasis.[5] Exclusively, the cationic form of the Zn (II) ion is found in systems of living organisms but at the cellular level it exists as inorganic or organic complexes controlling the concentrations of the free Zn (II) ion.[6] The common oxidation state of zinc in complexes is +2. It exhibits a coordination number of 4 as it obeys the 18-electron rule with such a configuration, but higher coordinated complexes have also been synthesized and reported.[7] Manganese is essential in biological processes of metabolism of oxygen molecules by the Manganese *catalase* and in enzymatic processes involving a group of enzymes, *phosphotransferases*.[8] The biological importance of nickel is related to its presence in metalloenzymes, but in the formation of its complexes, nickel (II) ions mostly exhibit octahedral coordination geometry. [9,10]

Thermogravimetric analysis and differential

scanning calorimetry provide information on the composition, thermal stability, and molecular structure of substances. Thermodynamics study of the TGA/DSC analysis gives relevant information on the bonding degree of ligand bound to metal ions and comparative ordered system between the reactants and the complexes.[11] For crystalline compounds, the PXRD analysis shows a diffraction pattern with sharp and well-defined peaks but narrow and significant. Reverse is the case for the amorphous compounds, where the PXRD pattern is rather smeared peaks with noise signals. When the ligands' XRD patterns are correlated with those of metal complexes of the same ligands, observation of new peaks suggests chelation.[12]

In the present study, mixed ligand metal complexes of 6-mercaptopurne and nicotinamide were synthesized by the one-pot synthetic method and characterized using FTIR, UV-Vis spectroscopy, elemental CHN analysis, PXRD, and thermogravimetric analysis. Molecular docking, density functional theory analysis (DFT), and *in vitro* antioxidant and antimicrobial activities were also carried out for the synthesized compounds.

2. Materials and Methods

Sigma Aldrich, Germany, is the source for the 6-mercaptopurne as well as nicotinamide ligands. The source of metal salts was British House Chemical Limited in England. Analytical - grade solvents were used throughout the experiment. All chemical reagents and solvents were used as received with no further purification.

2. 1 Synthesis of Metal-Ligand Complexes

A one – pot synthetic method was employed in the synthesis of the complexes with little modification .[13] 20 ml of ethanol/water or methanol/water was used to dissolve 1 mmol of metal salts. 1mmol (0.122 g) of nicotinamide and 1 mmol (0.170 g) of 6-mercaptopurine in 10 ml of hot ethanol were added to the metal salt solutions. The solutions obtained were stirred for 5 hours. The products obtained were filtered, washed in acetone, and air dried.

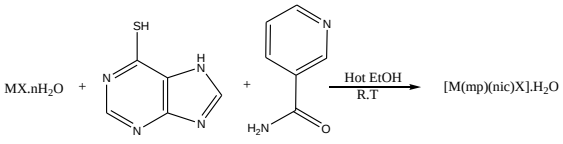

Scheme 1: Synthesis of Metal Complexes of 6-Mercaptopurine and Nicotinamide (M = Zn or Ni)

2.2 Characterization Methods

FLASH WA 1112 Series of CHN-Thermo Finnigan Italy was used to analyze the elemental composition of the complexes. A FTIR-8501 Shimadzu Spectrometer was used to record the FTIR spectra between 4000 and 400 cm^{-1}. At a 20 mL/min nitrogen gas flow rate and a temperature range of 25 to 1000 °C, the complexes were subjected to thermogravimetric analysis (TGA) using the TA SDT 650 instrument from Shimadzu. At a constant rate of 10 °C min^{-1}, about 5 mg of the solid samples were heated in an aluminum pan, sealed and non-hermetic. PXRD patterns were recorded on the EMPYREAN diffractometer system. The PXRD for the synthesized complexes of 6-mercaptopurine and nicotinamide were scanned and recorded in the range 2θ = 5.0287–79.9607° and at a wavelength, λ of 1.5406 Å.

2.3 Computational Studies and Docking Experiment - DFT calculations

2.3.1 DFT Analysis

The DFT computations were done for the Zn(mp)(nic)EtOH and [Ni(mp)(nic)(Ac)].4H_2O complexes. Compounds' structures were modeled with the aid of Avogadro software.[14] B3LYP functional with the 6–31G(d) basis set was utilized to ascertain the structures' geometry optimization. [15, 16] With ethanol as the solvent, the polarizable continuum solvation model (PCM) was also employed. B3LYP functionals in combination with the 6–31G(d) basis set have been reported to show better performance and are more suitable in determining electronic and thermochemical properties of several classes of compounds. [17-21] For the vibrational frequency calculations, using the time-dependent TD-DFT at the B3LYP/631-G(d) theoretical level, the electronic transitions of the optimized structures were explained [22, 23]. The solvent ethanol used for the recrystallization of the complexes in the experiment was also employed in the DFT calculations. The DFT calculations were used to evaluate the global molecular reactivity descriptors (GMRD) such as the energies of the lowest unoccupied molecular orbital (E_{LUMO}), highest occupied molecular orbital (E_{HOMO}), LUMO–HOMO energy gap (ΔE), chemical potential (μ), ionization energy (I), electrophilicity index (ω), global hardness (η), global softness (S) electron affinity (A), and electronegativity (χ). The chemical compounds' toxicity in terms of site selectivity and reactivity can be established through GMRD. [24–28] Two frontier orbitals, i.e., the LUMO and HOMO, are essential parameters for chemical behavior description.[29,30] The energy gap (ΔE), which explains a molecule's electrical transport characteristics, is mathematically expressed as the difference between E_{LUMO} and E_{HOMO}:

$$\Delta E = E_{LUMO} - E_{HOMO} \text{ -------} \quad (1)$$

The ionization energy and electron affinity are calculated using Koopman's theorem [31, 32] as:

$$A = -E_{LUMO} \text{ -------} \quad (2)$$

$I = -E_{HOMO}$ ------- (3)

The electronegativity (χ) can be calculated by taking the average of the ionization energy (I) and the electron affinity (A). [26, 33]

$$\chi = \frac{I+A}{2} \text{-------} \quad (4)$$

The electronegativity (χ) value is used to calculate the chemical potential (μ) as negative value.[31, 32-34]

$$\mu = -\chi = -\left(\frac{I+A}{2}\right) \text{-------} \quad (5)$$

The electrophilicity index (ω) of the molecule was determined from chemical potential (μ) and the global hardness (η) values using the expression.[31, 32, 35] :

$$\omega = \frac{\mu^2}{2\eta} \text{ -------} \quad (6)$$

The global hardness (η) was obtained from the electron affinity (*A*) and ionization energy (*I*) using the expression.[31, 32, 36]:

$$\eta = \frac{I-A}{2} \text{-------} \quad (7)$$

The global softness (*S*) which is the reciprocal of the global hardness (η) [31, 32, 37] was obtained as:

$$S = \frac{1}{\eta} \text{--------} \quad (8)$$

2.3.2: The Docking Experiment

The hypoxanthine–xanthine oxidase (H-XO) complex, which was used as the receptor with an experimental crystal structure referenced as PDB ID 3NRZ [38] , was downloaded from the repository of the Protein Data Bank (PDB) (http://www.rcsb.org.pdb), while, the structures for the standard drugs reported as potent inhibitors of xanthine oxidase; allopurinol [39] and febuxostat [40] , with reference Pubchem CIDs 135401907 and 134018, respectively were gotten from the repository of PubChem.[41]The hypoxanthine-xanthine oxidase experimental structure's water molecules and co-crystallized molecules were eliminated for the docking experiments, resulting in the free xanthine oxidase (XO), which serves as the receptor's initial structure (Figure. 2). The molecular modeling tool Auto-DockVina was employed for the analysis of the molecular docking experiments involving the two referenced ligands (allopurinol and febuxostat) and the two complexes Zn(mp)(nic)EtOH and [Ni(mp)(nic)(Ac)].4H_2O.[29] The receptor – ligand complexes were formed through successful targeted docking of each of the two referenced ligands and the two complexes with XO receptor[38] binding sites in the H-XO complex. The receptor–ligand interactions pattern and magnitude of the binding affinity were determined with reference to the AutoDock4 docking protocol.[42] The scoring function for the semi-empirical free energy force field, which indicates the ligand–receptor interaction's potential energy surface, was implemented with the LGA stochastic search method in the docking experiment.[43] A cut-off distance of 3.0 A was defined in the three Cartesian (*x*-, *y*-, and *z*-) directions around the binding site from the outermost atoms of the bounding simulation box of the XO receptor.

2.4. Biological Studies

2.4.1. Antimicrobial Study

Three bacteria were among the six microbial strains that were chosen for the antimicrobial investigation: *Pseudomonas aeruginosa, Staphylococcus aureus, and Escherichia coli,* and three fungi: *Candida albicans, Aspergillus niger, and Aspergillus flavus*. The agar diffusion method as reported in literature was employed in evaluating the antimicrobial study for the ligands and the complexes. Fluconazole and ciprofloxacin are the positive controls for the antifungal and antibacterial studies, respectively. The procedure was repeated in duplicate.

2.4.2 Antioxidant Study

The antioxidant potential of the complexes was evaluated with the DPPH (2,2-diphenyl-1-picrylhydrazyl)-free radical scavenging assay method. 0.02540 mM stock of the DPPH solution in absolute ethanol was prepared. 2 ml of each sample solution in absolute ethanol was shaken vigorously with an equivalent volume of DPPH solution (0.0254 mM) and incubated in the dark for 45 minutes. At 518 nm, the absorbance of each solution mixture was measured to determine the percentage inhibition. The app: www.ic50.tk was employed to determine the IC_{50} value for each complex. Solution of ascorbic acid in absolute ethanol was used as standard.

3. Results and Discussion

Selected physical properties and elemental composition analysis of the complexes are presented in **Table 1**.

Table 1: Physical Properties and Elemental Analysis of the Complexes

Complexes	Mol. Weight (g/mol)	Colour	Melting Point (°C)	Elemental Analysis: %found (%calc)		
				C	H	N
(1).[Zn(mp)(nic)(EtOH)]	383.8	White	317	41.51 (40.80)	2.74 (3.42)	21.11 (21.96)
(2).[Ni(mp)(nic)(Ac)].4(H_2O)	463.1	Greenish	322	32.95 (33.79)	2.62 (4.14)	17.77 (18.19)

Table 2: TGA/DSC Analysis of Zinc Metal Complex of 6-Mercaptopurine and Nicotinamide

Complex	Temperature Range (°C)	DTG Peak (°C)	% Weight loss Found (Calc.)	Loss Fragment/ No of Molecules
[Zn(mp)(nic)(EtOH)]	47 -197	111	10.3(11.5)	- (1EtOH)
	197 -700	416	69.0 (71.4)	- (mp + nic)
	700 - 989	--------	20.4 (21.1)	ZnO

Table 3: TGA/DSC Analysis of Nickel Metal Complex of 6-Mercaptopurine and Nicotinamide

Complex	Temperature Range (°C)	DTG Peak (°C)	% Weight loss Found (Calc.)	Loss Fragment No of Molecules
[Ni(mp)(nic)(Ac)]. 4(H_2O)	40 - 289	102	15.4 (15.5)	- (4 H_2O)
	289 - 927	497	45.0 (48.6)	- (nic + mp - SH)
	927 - 981	--------	31.1 (32.4)	- (Ac) + NiS

Table 4: Thermodynamics Activated Parameters of Zinc Metal Complex of 6-Mercaptopurine-Nicotinamide [Zn(mp)(nic)EtOH] and Nickel complex [Ni(mp)(nic)Ac].4H_2O

Compound	Stage	T_p (K)	E* (kJ/mol)	ΔS* (J/mol)	ΔH* (kJ/mol)	ΔG* (kJ/mol)
(1).[Zn(mp)(nic)EtOH]	First	452	53.16	- 176.71	1.80	81.63
	Second	681	4.03	-309.42	- 9.69	201.06
(2).[Ni(mp)(nic)Ac].4H_2O	First	375	49.14	-161.39	46.02	106.55
	Second	770	1.38	-319.68	-5.24	248.83

Table 5: Selected UV-Vis Spectra data of 6-Mercaptopurine-Nicotinamide Mixed Metal Complexes

Ligand/Complex	Medium	Wavelength(nm)	Assignment	Geometry
(1). [Zn(mp)(nic)(EtOH)]	DMF	270 313 331	π→ π* n→ π* LMCT	Tetrahedral
(2).[Ni(mp)(nic)(Ac)].4H_2O	DMF	275 307 375	π→ π* n→ π* LMCT	Square planar

Table 6: Global molecular descriptors of the Synthesized complexes obtained from DFT calculations

Parameters (eV)	Zn comp (g)	Zn comp (sol)	Ni comp (g)	Ni comp (sol)
E_{HOMO}	-5.369	-5.606	-5.861	-6.116
E_{LUMO}	-2.038	-2.351	-4.632	-5.087
ΔE (E_{LUMO} - E_{HOMO})	3.331	3.255	1.229	1.029
I	5.369	5.606	5.861	6.116
A	2.038	2.351	4.632	5.087
η	1.666	1.628	0.615	0.515
S	0.600	0.614	1.627	1.944
χ	3.704	3.979	5.247	5.602
μ	-3.704	-3.979	-5.247	-5.602
ω	11.422	12.880	8.457	8.072

The mixed ligand metal complexes have melting points higher than the melting points of the ligands, nicotinamide and 6-mercaptopurine (128 and 313 °C, respectively) showing that there is coordination of the metals and mixed ligands, 6-mercaptopurine and nicotinamide, and the compounds have good thermal stability.[44] The solvent ethanol partakes in the formation of the compounds **(1),** while compound **(2)** has characteristic uncoordinated water molecules outside the coordination sphere. Compound **(1)** is a whitish powder, while compound **(2)** is greenish in colour. The transition metals with vacant orbitals have characteristic colour on forming a complex due to available vacant orbitals and possible transitions except zinc with completely filled d-subshell orbitals. The elemental CHN analysis of the complexes is in good correlation with the experimental value supporting the formation of the complexes.

3.1.2 FTIR Analysis of the Complexes

The FTIR spectra of the complexes **(1)** and **(2)** are found on supplementary files X1 and X2, respectively. The band at 1617 and 1614 cm^{-1} assigned to the deformation on the pyrimidine ring in the 6-mercaptopurine and nicotinamide had shifted to 1603 cm^{-1} in the spectra of the zinc compound **(1)** upon complexation. This implies the participation of the pyrimidine ring in the formation of the complex, and similar coordination modes were reported.[45] The sulphur exocyclic (S-6) atom on the pyrimidine coordinated the central zinc metal as indicated by a shift of the -C=S band from 1222 to about 1202 cm^{-1} coupled with a decrease in intensity. Participation of the imidazole ring in the complexation is also indicated by a shift in the band 1409 cm^{-1} assigned to the deformation of the imidazole ring to 1440 cm^{-1}. The nicotinamide coordinated to the central zinc metal in compound **(1)** through the nitrogen of the pyridinic ring. Similar coordination mode was observed for the other complex, but the compound **(2)** of nickel metal-6-mercaptopurine and nicotinamide complex IR spectra shows a broad peak in the region 3552–3200 cm^{-1} assigned to uncoordinated water molecules. [46 - 47] New peaks in the fingerprint region 437 to about 555 cm^{-1} suggest metal–ligand coordination in the complexes.

3.1.3 TGA and Thermodynamic Parameters Analysis of the Complexes

Thermogravimetric analysis results of compound (1) are presented on Table 2, while the thermal decomposition, pattern is shown on Figure 1. Compound **(1)** shows two stages of thermal decompositions with the final step involving the formation of an oxide of zinc metal. The first stage is the loss of one molecule of ethanol with 11.5% calculated weight loss 10.3% found. The stage is an endothermic decomposition process at a peak temperature of 111 °C. The second stage of decomposition involves simultaneous loss of the ligands, 6-mercaptopurine and nicotinamide, with a calculated percentage loss of 71.4% (69.0% found). The second stage of decomposition was inferred as an exothermic process at a peak temperature of 415.9 °C. The calculated moiety loss at various stages is consistent with the proposed compositions of the compound.[48] The thermal decomposition pattern of compound **(2)** [Ni(mp)(nic)(Ac)].4H_2O (**Table 3; Figure 2**), indicates the loss of four uncoordinated water molecules in the first stage, with 15.4% wt loss found against 15.5% wt loss calculated. The second stage in the temperature range of 289 to 927 °C is an exothermic simultaneous elimination of the mixed ligands, with 45.0% wt loss found and 48.6% wt loss calculated. The decomposition process becomes constant at a temperature of about 927 °C, involving residual formation of the metal sulphide and elimination of the coordinated acetate group.

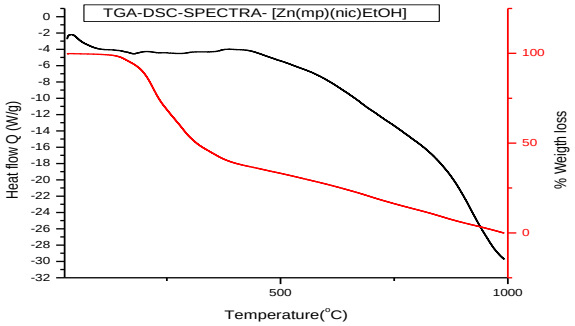

Figure 1: Thermal Decomposition Pattern Curve for Zinc Metal Complex of 6-Mercaptopurine and Nicotinamide

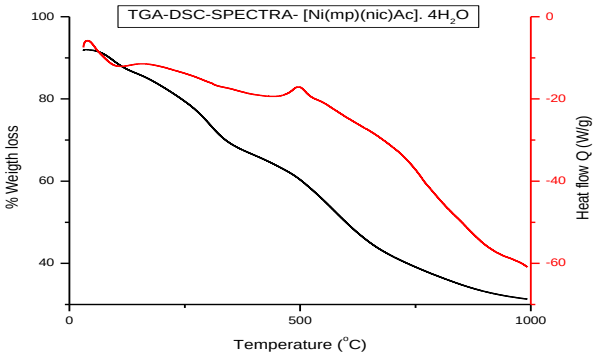

Figure 2: Thermal Decomposition Pattern Curve for Nickel Metal Complex of 6-Mercaptopurine and Nicotinamide

The thermodynamics activated parameters: activation energy, enthalpy change, entropy, and Gibb's free energy change for the compounds **(1) and (2)** are listed on **Table 4**. The activated parameters were obtained from the data of the thermal decomposition curve coupled with the *Coat - Redfern* equation.[49, 50] A plot of log Q against $\frac{1}{T}$ was obtained for each stage of decomposition; activation energy was estimated using the value of the slope, while frequency factor Z was estimated from the intercept.

$$\log\left[\frac{log\left(\frac{W_f}{W_f - W}\right)}{T^2}\right] = \log\left[\frac{ZR}{\theta E^*}\left(1 - \frac{2RT}{E^*}\right)\right] - \frac{E^*}{2.303RT}$$

Equation 1: *Coat- Redfern* equation where log Q represent the L.H.S expression of the equation.

Mass loss at the completion of the reaction is W_f , mass loss up to temperature T is W; R is the gas constant, activation energy in kJ/mol is E*, θ is the heating rate while the expression (1- (2RT/E*) ≈ 1.

The numerical activation energy, E*, for the first and second stage decomposition of compound **(1)**, [Zn(mp)(nic)EtOH] were evaluated from the slope of the curves, **Figures 3 and 4**, with values of -2776.60 and 210.264, respectively. The activation energies determined are 53.16, and 4.03 kJmol^{-1}, respectively, while the entropy of activation, -176.71 and -309.42 Jmol^{-1}, are evaluated for the first and second stages of decomposition, respectively. Activation energy being positively high and the entropy of activation being negative is an indication that the complex is stable and has a more ordered structure than the ligands, which is supported by the high positive values of the activated Gibb's free energy change. Also the thermal decomposition of the compound **(1),** [Zn(mp)(nic)EtOH], is accompanied by the appearance of endothermic and exothermic peaks, as indicated by the activated enthalpy change ΔH* values of 1.80 and -9.69 kJmol^{-1} for stages one and two respectively, (**Table 4**). Similar results were reported by Chaudhary and Mishra[51] for mixed ligand metal complexes of streptomycin and amoxicillin with negative values for entropy of activation and higher activation energy in the range 16.58– 114 Jmol^{-1}. Compound **(2)** also shows high values for the activation energy, which implies stability of the complex as it undergoes the two stages of decomposition, but the negative entropy values for the two stages shows the compound to possess a more ordered structure compared to the reactants.[52] The evaluated ΔH* negative value for the second stage of decomposition supports the exothermic process, as the exothermicity is not compensated for by the energy heat of degradation released during the process. The higher activated Gibb's free energy change values for the two stages support the more ordered nature of the compounds compared to the ligands, and degradation of the compound is therefore nonspontaneous (**Table 4**).

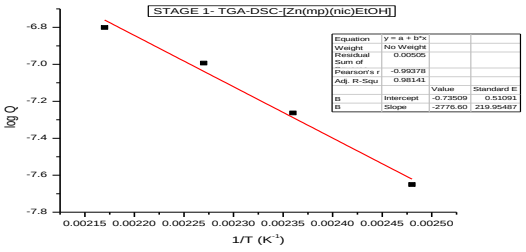

Figure 3: Plot of logQ against 1/T for stage 1 TGA Decomposition of [Zn(mp)(nic)(EtOH)]

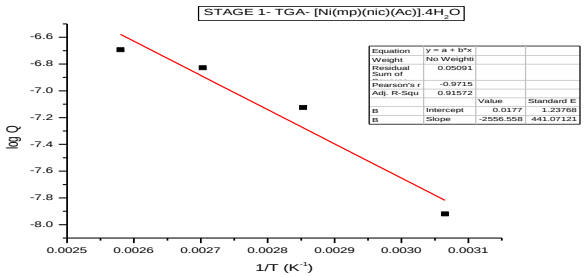

Figure 4: Plot of logQ against 1/T for stage 1 TGA Decomposition of [Ni(mp)(nic)(Ac)].4H$_2$O

3.1.4 UV-Vis Spectra Analysis of the Complexes

The compound **(1)**, which is a zinc metal complex, has intraligand transitions at 270 nm and 313 nm, but the observed band at 331 nm can be assigned to the ligand metal charge transfer transition (**Table 5**). Three major bands in the region 230–390 nm are typically observed for Zn (II) complexes. The compound shows no *d* → *d* transition as expected for the d^{10} configuration of Zn(II) compounds; the compound is therefore proposed as a tetrahedral complex (**Figure 5**), while the compound **(2)** of the nickel metal complex UV-Vis spectrum shows two bands at 307 and 375 nm transition, which are assigned to n→π* and LMCT, respectively, therefore proposed as a square – planar geometry nickel complex (**Figure 6**).[53]

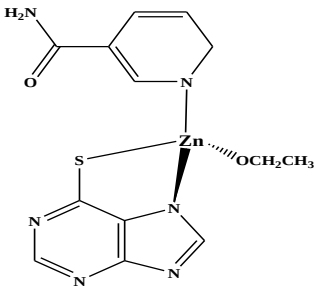

Compound (1): [Zn(mp)(nic)EtOH]

Figure 5: Proposed Structure of Compound (1), [Zn(mp)(nic)EtOH]

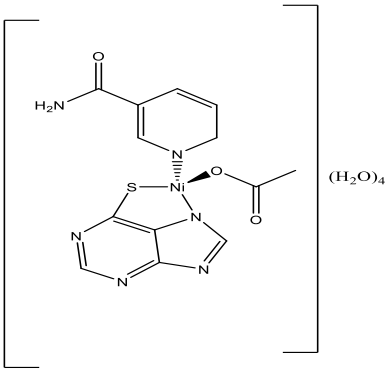

Figure 6: Proposed Structure of Compound (2), [Ni(mp)(nic)(Ac)].4H$_2$O

3.1.5 PXRD Analysis of the Complexes

Sharp crystalline peaks are observed for the X-ray diffractogram patterns of compound **(1)** [Zn(mp)(nic)EtOH]**,** showing its crystalline phase to be better than compound **(2) (Figures 7 and 8**)**.** A similar report on crystallinity was reported by Khan[54] for zinc (II) complexes having sharp peaks with line broadening. While the sharp peaks suggest higher crystallinity of the complex**,** the line broadening indicates incorporation of water molecules in the structure of the complex. The absence of peaks with line broadening in compound **(1)** suggesting no water molecule in the structure of this compound compared to the X-ray diffractogram patterns of compound **(2)** with line broadening peaks indicates incorporation of water molecules in the structure of the complex.

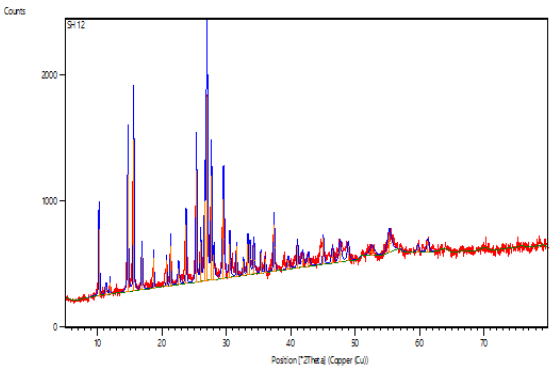

Figure 7: PXRD Diffractograms Pattern for Compound (1), [Zn(mp)(nic)EtOH]

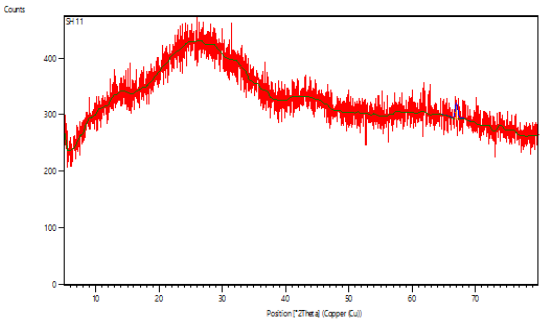

Figure 8: PXRD Diffractogram Pattern for Compound (2), [Ni(mp)(nic)(Ac)].4H_2O

3.2 Results of Computational Studies and Docking Experiment

3.2.1 DFT Results

The results of the chemical reactivities of the Zn(mp)(nic)EtOH and [Ni(mp)(nic)(Ac)].4H_2O complexes in the gas phase and ethanol from the DFT study computed in terms of the global molecular reactivity descriptors were shown on **Table 6**. Lower values of (E_{LUMO} *and* E_{HOMO}), global softness (S), and chemical potential (μ), as well as the correspondingly higher values of global hardness (η), ionization energy (I), electronegativity (χ), and electrophilicity index (ω), suggest significant effect of the presence of solvent in the formation of Zn(mp)(nic)EtOH and [Ni(mp)(nic)(Ac)].4H_2O complexes. The LUMO–HOMO energy gap (ΔE) values for Zn(mp)(nic)EtOH and [Ni(mp)(nic)(Ac)].4H_2O complexes in ethanol medium are 3.255 eV and 1.029 eV, respectively. The [Ni(mp)(nic)(Ac)].4H_2O complex which is a d^8 system, has a lower ΔE value than the Zn(mp)(nic)EtOH complex, a d^{10} system. This is likely due to the occurrence of additional *d-d* transitions within the Ni(II) metal ion, which confers extra stability on the complex. The [Ni(mp)(nic)(Ac)].4H_2O has lower values of global hardness and chemical potential than that of Zn(mp)(nic)EtOH. Energy gap and global hardness have relatively lower values, suggesting that the [Ni(mp)(nic)(Ac)].4H_2O complex is a softer molecule than Zn(mp)(nic)EtOH with lower kinetic stability but higher chemical reactivity; higher electro-optic response indicated that it is more magnetisable and polarizable.[55, 56] The optimized structures of the complexes are shown in **Figure 9**. The surface plots for the energy gap between the frontier orbitals (LUMO–HOMO) of Zn(mp)(nic)EtOH and [Ni(mp)(nic)(Ac)].4H_2O complexes are displayed in **Figure 10**. For the frontier orbitals, the HOMO are primarily electron donors, while LUMO are electron acceptors. The degrees of chemical stability of molecules are a function of the energy gap between LUMO and HOMO.[57] In the Zn(mp)(nic)EtOH complex, the surface plot of the LUMO showed that electron density is majorly distributed on the nicotinamide ligand, while for the HOMO, the electron density is distributed mainly on the 6-mercaptopurine ligand. Thus, the main bonding and anti-bonding electrons for the formation of the Zn (II) complex are from electron donor atoms of the 6-mercaptopurine ligand and the electron acceptor atoms of nicotinamide ligand, respectively. Similarly, for the [Ni(mp)(nic)(Ac)].4H_2O complex, the surface plot of the LUMO revealed that the electron density is majorly distributed on the nicotinamide ligand and the nickel and carboxyl oxygens of the acetate, while for the HOMO the electron density is distributed mainly on the 6-mercaptopurine ligand.

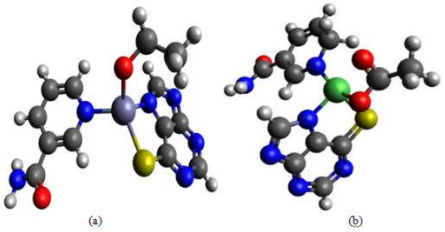

Figure 9: The optimized structures of (a) Zn(mp)(nic)EtOH and (b) [Ni(mp)(nic)(Ac)].4H_2O

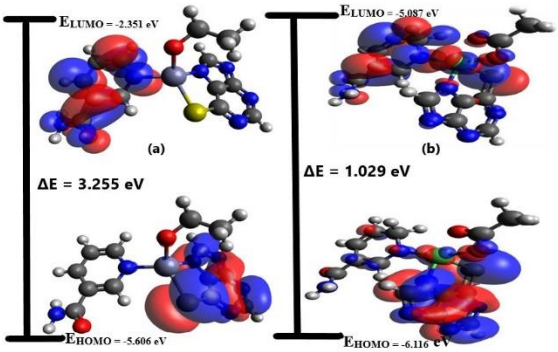

Figure 10: Surface plots of the Energy gap (LUMO–HOMO) for (a) Zn(mp)(nic)EtOH complex and (b) Ni(mp)(nic)(Ac) complex

3.2.2 Molecular Docking Results

Antioxidants prevent oxidative stress that causes deadly diseases such as cancer. Some substances, when ingested, inhibit Xanthine oxidase (XO), thereby preventing uric acid from generating reactive oxygen species (ROS). Such substances are therefore regarded as potent exogenic antioxidants. The purine based inhibitors are allopurinol, oxypurinol, and tisopurinol, while non-purine-based inhibitors are topiroxostat, febuxostat, and inositols. [58] [59] These are the two classes of XO inhibitors, each acting on two different binding pockets (I and II) of the XO. The free Xanthine oxidase cartoon and surface representations are shown in **Figure 11**. Results from our molecular docking studies, as shown in **Figure 12,** revealed that only the Zn(mp)(nic)EtOH complex docked at one of the active sites of XO, the purine-based inhibitor binding pocket, while the [Ni(mp)(nic)(Ac)].4H_2O complex docked at position different from the two binding pockets of xanthine oxidase. Therefore, it can be concluded that the [Ni(mp)(nic)(Ac)].4H_2O complex is not likely to possess antioxidant property since it does not bind at any of the two active binding sites of xanthine oxidase and thus lacks the potential to act as an xanthine oxidase inhibitor. On the other hand, the Zn(mp)(nic)EtOH complex, which docked alongside allopurinol at binding pocket I with a binding affinity value of -6.4 kcal mol^{-1}, showed antioxidant potential. It is also worthy to note that the binding affinity of -6.4 kcal mol^{-1}, for Zn(mp)(nic)EtOH is lower than that of allopurinol (− 5.3 kcal mol^{-1}). The findings from this docking experiment agree perfectly with experimental findings that Zn(mp)(nic)EtOH complex possesses good antioxidant potential.

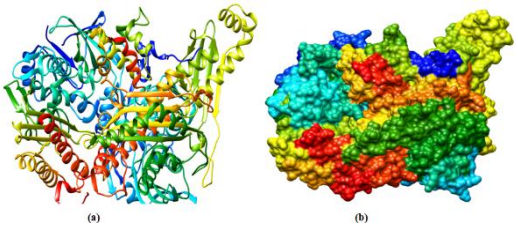

Figure 11: The free Xanthine oxidase (a) cartoon representation, (b) surface representation

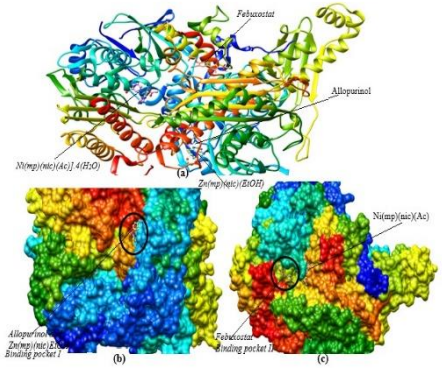

Figure 12: Inhibitors docked in Xanthine oxidase (a) cartoon representation of inhibitors docked in XO, (b) surface representation of XO showing binding pocket I with Allopurinol and Zn(mp)(nic)EtOH docked inside the pocket and (c) surface representation of XO showing binding pocket II with Ni(mp)(nic)(Ac) docked outside the pocket.

3.3 Results of Biological Activity of the Complexes

3.3.1 Antimicrobial Studies of 6-Mercaptopurine-Nicotinamide Mixed Metal Complexes

Antimicrobial activity of the mixed 6-mercaptopurine and nicotinamide synthesized complexes is shown in **Figures 13 and 14**. The compounds generally show a remarkable increase in antibacterial activity against the three bacterial strains, *Pseudomonas aeruginosa (Pseudo), Escherichia coli (E-coli), and Staphylococcus aerues (Staph aerues)*. Compound **(2)** [Ni(mp)(nic)(Ac)].4H_2O shows the strongest activity against *Pseudomonas aeruginosa* compared to the ligand 6-mercaptopurine and the ciprofloxacin positive reference standard; **Figure 13**.

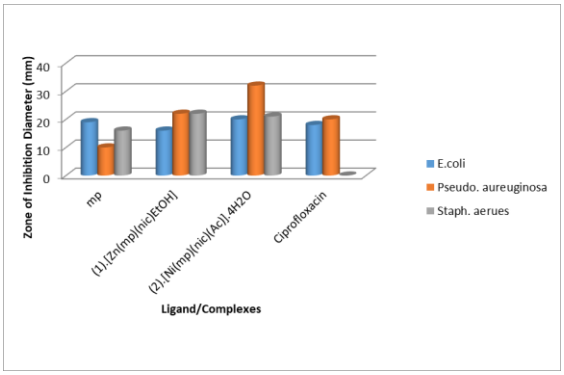

Figure 13: Antibacterial Activity of Mixed 6-Mercaptopurine-Nicotinamide Metal Complexes

The antifungal activity of the metal complexes is shown in **Figure 14**, indicating the zone of inhibition against the fungal strains, *aspergillus flavus, aspergillus niger, and candida albicans*. Compound **(1)** shows no inhibition against *candida albicans,* while compound **(2)** of the nickel (II) metal complex shows moderate inhibition against *candida albicans*. The compounds only show moderate inhibition against *aspergillus niger and aspergillus flavus*. The observed improved antimicrobial activity of the compounds can be explained through the chelation theory also supported by the lipophilicity concept. When the metal ion chelates the ligands, polarity of the metal atom is diminished because of partial sharing of its positive charge with the donor atoms of the ligands and delocalization of the π-electrons on the rings of the ligands. This facilitates the lipophilicity of the metal complexes and eases the permeation through the lipid layers of the cell membrane and inhibits further growth of the organisms, but the cell membranes with characteristic lipopolysaccharides in the outer membrane as observed in the structures of Gram-negative bacteria can explain the improved antibacterial activity against *Pseudomonas aeruginosa*.[60]

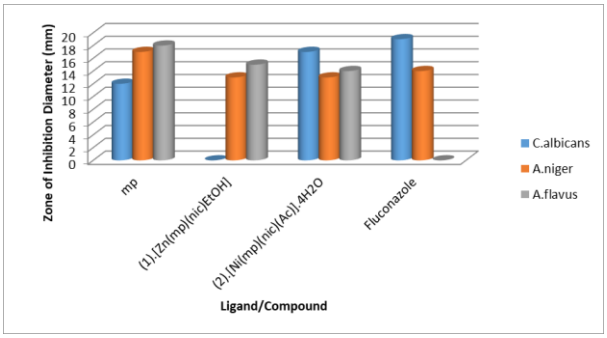

Figure 14: Antifungal Activity of Mixed 6-Mercaptopurine-Nicotinamide Metal Complexes

3.3.2 Antioxidant Study of 6-Mercaptopurine-Nicotinamide Mixed Metal Complexes

The compound **(1)** shows antioxidant percentage inhibition against DPPH less than ascorbic acid of similar concentrations but better than the ligand 6-mercaptopurine, while compound **(2)** of nickel metal mixed 6-mercaptopurine and nicotinamide shows the lowest percentage inhibition of 57.17% at a concentration of 0.05 mg/ml (**Figure 15**). The IC_{50} values determined are presented in **Figure 16** for compounds **(1) and (2).** Compound **(1)** of the zinc (II) metal complex shows the lowest IC_{50} of 0.58, which suggests its effectiveness as an antioxidant agent. The presence of organic moiety, ethanol, and the enzymatic nature of zinc metal in the structure of compound **(1),** can explain the lowest IC_{50} value of 0.58 for the compound **(1)** which implies its effectiveness as an antioxidant agent, unlike the lowest antioxidant percentage inhibition reported for the compound **(2)** with four uncoordinated water molecules.[61] The mechanism of antioxidant activity for the compounds can be explained by the fact that the DPPH solution receives electrons from the synthesized metal complexes, i.e., the antioxidant, which brings about colour change, and the free-radical scavenging is inversely related to the absorbance of the resultant solution measured. Other structural factors of compounds that affect their antioxidant activity are the presence of functional groups like carboxylic groups and phenolic hydroxyl groups.[61, 62]

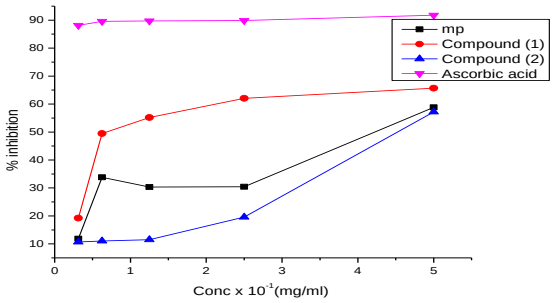

Figure 15: Percentage Inhibition of Mixed6-Mercaptopurine-Nicotinamide Metal Complexes against DPPH Solution

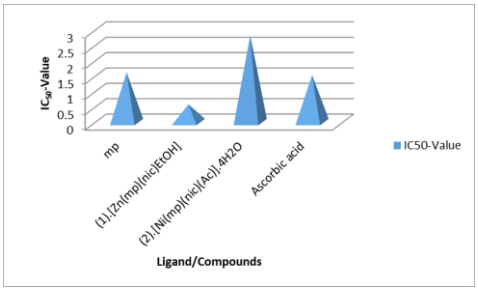

Figure 16: IC_{50}- Values of Mixed 6-Mercaptopurine-Nicotinamide Metal Complexes.

4. Conclusion

We have successfully synthesized mixed-ligand metal complexes of 6-mercaptopurine-nicotinamide. 6-mercaptopurine acts as bidentate ligand while nicotinamide acts as monodentate ligand in the formation of the compounds **(1)** [Zn(mp)(nic)EtOH] and **(2)** [Ni(mp)(nic)(Ac)].4H_2O. Supporting the spectroscopic analysis is the computational study's report for the Zn(mp)(nic)EtOH complex. The electron density of the LUMO is primarily distributed on the nicotinamide ligand, but the electron density of the HOMO is smeared majorly on the 6-mercaptopurine ligand. Compound **(1)** [Zn(mp)(nic)EtOH] is a better antioxidant agent compared to compound **(2)** [Ni(mp)(nic)(Ac)].4H_2O, but compound **(2)** shows improved antimicrobial activity compared to compound **(1)**. The findings from the docking experiment are in agreement with the experimental results on the positive antioxidant potential of the Zn(mp)(nic)EtOH complex **(1),** which docked alongside allopurinol at binding pocket I with a binding affinity value of -6.4 kcal mol^{-1}, showing its antioxidant potential.

Author contributions

Sheriff O. Ayinla: Conceptualization, design, and manuscript first draft. **Abdullah O. Rajee:** results analysis and manuscript revision; **Kamil O. Yusuff**: data curation and DFT analysis; **Ginikachukwu G. Mbaeyi**: resources and editing; **Hassan K. Busari:** manuscript revision and proofreading; **Joshua A. Obaleye:** manuscript revision and project supervision.

Conflict of interest

The authors declare no conflict of interest.

Acknowledgements

The authors wish to acknowledge the Centre for High Performance Computing (CHPC) of the Council for Scientific and Industrial Research (CHPC-CSIR, South Africa) for access to computing resources used to perform computational aspects of this work.

References

1. Sharfalddin, A. A.; Emwas, A. H.; Jaremko, M.; Hussien, M. A. Complexation of Uranyl $(UO_2)^{2+}$ with Bidentate Ligands: XRD, Spectroscopic, Computational, and Biological Studies. *PloS one*. **2021**, 16(8), e0256186.
2. Aseman, M. D.; Aryamanesh, S.; Shojaeifard, Z.; Hemmateenejad, B.; Nabavizadeh, S. M. Cycloplatinated (II) Derivatives of Mercaptopurine Capable of Binding Interactions with HSA/DNA. *Inorganic Chemistry* **2019**, 58(23), 16154-16170.
3. Al-Noor, T. H.; Mohapatra, R. K.; Azam, M.; Karem, L. K. A.; Mohapatra, P. K.; Ibrahim, A. A.; ... Pintilie, L. Mixed-Ligand Complexes of Ampicillin Derived Schiff Base Ligand And Nicotinamide: Synthesis, Physico-Chemical Studies, DFT Calculation, Antibacterial Study and Molecular Docking Analysis. *Journal of Molecular Structure* **2021**, 1229, 129832.
4. Akinyele, O. F.; Fakola, E. G.; George, R. C.; Durosinmi, L. M. Synthesis, Characterization and Antibacterial Activity of Mixed Ligand Complexes of Nicotinamide and 2, 2′-Bipyridine. *Ife Journal of Science* **2021**, *23*(1), 213-222.
5. Clemens, S. Metal Ligands in Micronutrient Acquisition and Homeostasis. *Plant, Cell & Environment* **2019**, 42(10), 2902-2912.
6. Mirbolook, A.; Rasouli-Sadaghiani, M.; Sepehr, E.; Lakzian, A.; Hakimi, M. Synthesized Zn (II)-Amino Acid and-Chitosan Chelates to Increase Zn Uptake By Bean (Phaseolus Vulgaris) Plants. *Journal of Plant Growth Regulation* **2021**, 40, 831-847.
7. Hammond, M.; Rauch, M.; Parkin, G. Synthesis, Structure, and Reactivity of a Terminal Cadmium Hydride Compound,[κ3-TismPriBenz] CdH. *Journal of the American Chemical Society* **2021**, 143(28), 10553-10559.
8. Gao, T.; Ding, M.; Yang, C. H.; Fan, H.; Chai, Y.; Li, Y. The Phosphotransferase System Gene Ptsh Plays an Important Role in Mnsod Production, Biofilm Formation, Swarming Motility, and Root Colonization in Bacillus Cereus 905. *Research in microbiology* **2019**, 170 (2), 86-96.
9. Alfano, M.; Cavazza, C. Structure, Function, and Biosynthesis Of Nickel-Dependent Enzymes. *Protein Science* **2020**, 29(5), 1071-1089.
10. Khursheed, S.; Siddique, H. R.; Tabassum, S.; Arjmand, F. Water Soluble Transition Metal [Ni (II), Cu (II) and Zn (II)] Complexes of N-Phthaloylglycinatebis (1, 2-diaminocyclohexane). DNA Binding, pBR322 Cleavage and Cytotoxicity. *Dalton Transactions* **2022**, 51(31), 11713-11729.
11. Odedra, P.; and Rojivadiya, A. J. Synthesis and Characterization of Transition Metal Complexes of Some Novel Pyrazolo-Chalcone Derivatives. *World Scientific News*, **2019**, 131, 242-255.
12. Fathima, S.; Meeran, M.; Nagarajan, E. R. Synthesis, Characterization and Biological Evaluation of Novel 2, 2′-((1, 2-Diphenylethane-1, 2-Diylidene) Bis (Azanylylidene)) Bis (Pyridin-3-Ol) and Metal Complexes: Molecular Docking and in Silico

ADMET Profile. *Structural Chemistry*, **2020**, 31(2), 521-539.
13. Rathi, Anuj K.; Manoj B.; Gawande, Radek Zboril.; Rajender S. Varma. "Microwave-Assisted Synthesis–Catalytic Applications in Aqueous Media." *Coordination Chemistry Reviews*, **2015**, 291, 68-94.
14. Marcus, D. H.; Donald, E. C.; David, C. L.;, Tim, V.; Eva, Z.; Geoffrey, R. H. "Avogadro: An Advanced Semantic Chemical Editor, Visualization, And Analysis Platform" . *Journal of Cheminformatics*, **2012**, 4, 17.
15. Becke, A. D. *J. Chem. Phys*. **1993**, 98, 5648 .
16. Lee C.; Yang. W.; Parr.G. R. *Phys. Rev.* **1998**, 37, 785 .
17. Riley, E K.E.; Op'tHolt, B.T.; Merz, K.M. *J. Chem. Theory Comput*. **2007**, 3, 407 .
18. Tirado-Rives, J.; Jorgensen, W.L.; *J. Chem. Theory Comput*. **2008,** 4, 297.
19. Hassan, H. B. Density function theory B3LYP/6–31G** Calculation of Geometry Optimization and Energies of Donor-Bridge Acceptor Molecular System. *Int J Curr Eng Sci Res*. **2014**, 4, 2342–2345.
20. Nascimento, D. R.; Biasin, E.; Poulter, B. I.; Khalil, M.; Sokaras, D.; Govind, N. Resonant Inelastic X-Ray Scattering Calculations of Transition Metal Complexes Within A Simplified Time-Dependent Density Functional Theory Framework. *J Chem Theory* Comput. **2021**, 17(5), 3031–3038.
21. Barhoumi, A.; Zeroual, A.; Bakkas, S.; El Hajbi, A. Theoretical Study Of The Regioselectivity Of The Reaction Between Tetrachloromethane And Triethylphosphite Using the DFT B3LYP/6-31G(d) Method. *J Comput Methods Mol Des.* **2015** 5(2) , 8–15
22. Runge, E.K.G. *Phys. Rev*. **1984** B. 52, 997.
23. Nakatsukasa, T.; Matsuyanagi, K.; Matsuo, M.; Yabana, K. Time-Dependent Density-Functional Description of Nuclear Dynamics. *Rev Mod Phys*. **2016** , 88(4), 045004.
24. Parthasarathi, R.; Padmanabhan, J.; Subramanian, V.; Sarkar, U.; Maiti, B.; Chattaraj, P. Toxicity Analysis of Benzidine Through Chemical Reactivity and Selectivity Profiles: A DFT Approach. *Int. Electron J Mol*. **2003**, 2, 798–813.
25. Parthasarathi, R.; Padmanabhan, J.; Subramanian, V.; Sarkar, U.; Maiti, B.; Chattaraj, P. Intermolecular Reactivity through the Generalized Philicity Concept. *Chem Phys Lett*. **2004a**, 394, 225–230.
26. Talmaciu, M. M.; Bodoki, E.; Oprean, R. Global Chemical Reactivity Parameters for Several Chiral Beta-Blockers from the Density Functional Theory Viewpoint. *Clujul Med*. **2016**, 89(4), 513.
27. Parthasarathi, R.; Padmanabhan, J.; Subramanian, V.; Sarkar, U.; Maiti, B.; Chattaraj, P. Toxicity Analysis of 33'44'5-Pentachloro Biphenyl through Chemical Reactivity and Selectivity Profiles. *Curr. Sci*. **2004b**, 86, 535–542.
28. Molski, M. Theoretical Modelling Of Structure-Toxicity Relationship Of Cyanides. *Toxicol. Lett*. **2021**, 349, 30–39.
29. Shoba, D.; Periandy, S.; Karabacak, M.; Ramalingam, S. *Spectrochim. Acta* A, **2011**, 83, 540.
30. Khalid, M.; Ullah, MA.; Adeel, M.; Khan, M.U.; Tahir, M. N.; Braga, A. A. C. Synthesis, Crystal Structure Analysis, Spectral IR, UV–Vis, NMR Assessments, Electronic And Nonlinear Optical Properties of Potent Quinoline Based Derivatives: Interplay of Experimental and DFT Study. *J. Saudi Chem. Soc*. **2019**, 23(5), 546–560.
31. Koopmans, T. *Physica*, **1934**, 1, 104.
32. Abdulaziz, H.; Gidado, A. S.; Musa, A.; Lawal, A. Electronic Structure and Non-Linear Optical Properties of Neutral and Ionic Pyrene and Its Derivatives Based on Density Functional Theory. *J. Mater Sci Res Rev*. **2019**, 2(3), 1–13.
33. Mulliken, R.S. *J. Chem. Phys*. **1934**, 2, 782–793.
34. Parr, R.G.; Donnelly, R.A.; Levy, M.;. Palke, W.E. *J. Chem. Phys*. **1978**, 68, 381.
35. Parr, R.G.; Szentpaly, L.V.; Liu, S. *J. Am. Chem. Soc*. **1999a**, 121, 1922.
36. Parr, R.G.; Pearson, R.G. *J. Am. Chem. Soc.* **1983b**, 105, 7512.
37. Yang, W.; Parr, R.G. *Proc. Natl. Acad. Sci*. **1985**, 82, 6723.
38. Cao, H.; Pauff, J.M.; Hille, R. Substrate Orientation and Catalytic Specificity in the Action of Xanthine Oxidase the Sequential Hydroxylation of Hypoxanthine to Uric Acid. *J Biol.Chem*. **2010**, 285, 28044–28053.
39. Love, B. L.; Barrons, R.; Veverka, A.; Snider, K. M. Urate Lowering Therapy for Gout: Focus on Febuxostat. *Pharmacotherapy*. **2010**, 30, 594–608.
40. Kim, S.; Chen, J.; Cheng, T.; Gindulyte, A.; He, J.; He, S.; Li, Q.; Shoemaker, B. A.; Thiessen, P. A.; Yu, B.; Zaslavsky, L.; Zhang, J.; Bolton, E. E. improved access to chemical data.Nucleic Acids. *PubChem* 2019 update. **2019**, Res 47, D1102–D1109.
41. Trott, D.; Olson, A. J. AutoDockVina: Improving the Speed and Accuracy of Docking With a Scoring Function, Efficient Optimization and Multithreading. *J ComputChem*. **2010**, 31, 455–461.
42. Morris, G. M.; Huey, R.; Lindstrom, W.; Sanner, M. F.; Belew, R. K.; Goodsell, D. S.; Olson, A. J. Autodock4 and AutoDockTools4: Automated Docking with Selective Receptor Flexibility. *J ComputChem*. **2009**, 30, 2785–2791.

43. Morris, G. M. Automated Docking Using a Lamarckian Genetic Algorithm and Empirical Binding Free Energy Function. *J ComputChem*. **1998**, 19, 1639–1662.
44. Akinyele, O. F.; Fakola, E. G.; George, R. C.; Durosinmi, L. M. Synthesis, Characterization and Antibacterial Activity of Mixed Ligand Complexes of Nicotinamide and 2, 2′-Bipyridine. *Ife Journal of Science*. **2021**, *23*(1), 213-222.
45. Hang, N. T. N.; Si, N. T.; Nguyen, M. T.; Nhat, P. V. Adsorption/Desorption Behaviors and Sers Chemical Enhancement of 6-Mercaptopurine on a Nanostructured Gold Surface: the Au20 Cluster Model. *Molecules*. **2021**, 26(17), 5422.
46. Sharma, P.; Gogoi, A.; Verma, A. K.; Frontera, A.; Bhattacharyya, M. K. Charge-Assisted Hydrogen Bond And Nitrile··· Nitrile Interaction Directed Supramolecular Associations In Cu (II) And Mn (II) Coordination Complexes: Anticancer, Hematotoxicity and Theoretical Studies. *New Journal of Chemistry*. **2020**, *44*(14), 5473-5488.
47. Kumar, R.; Singh, R. K.; Shankar, R. Critical Success Factors for Implementation of Supply Chain Management in Indian Small and Medium Enterprises and their Impact on Performance. *IIMB Management review*. **2015**, 27(2), 92-104.
48. Karapınar, E.; Gubbuk, I. H.; Taner, B.; Deveci, P.; Ozcan, E. Thermal Degradation Behaviour of Ni (II) Complex of 3, 4-Methylenedioxaphenylaminoglyoxime. *Journal of Chemistry*. **2013**, 2013(1), 548067.
49. Shelke, V. A.; Jadhav, S. M.; Shankarwar, S. G.; Munde, A. S.; Chondhekar, T. K. Synthesis, Characterization, Antibacterial and Antifungal Studies of Some Transition and Rare Earth Metal Complexes of N-Benzylidene-2-Hydroxybenzohydrazide. *Bulletin of the Chemical Society of Ethiopia*. **2011**, 25(3), 381-391.
50. Al-Duhaidahawi, D. L.; Jabir, M. S.; Al-Amiery, A. A. Moneim, A. E. A.; Alkaim, A. F., Kadhum, A. A. H. Novel Antioxidants Compounds Derived from Isatine. *Biochem. Cell. Arch*. **2018**, 18(1), 709-713.
51. Chaudhary, N. K.; Mishra, P. In Vitro Antimicrobial Screening of Metal Complexes of Schiff Base Derived from Streptomycin and Amoxicillin: Synthesis, Characterization and Molecular Modelling. *American Journal of Applied Chemistry*, **2014**, *2*(1), 19-26.
52. Shelke, V. A.; Jadhav, S. M.; Patharkar, V. R.; Shankarwar, S. G.; Munde, A. S.; Chondhekar, T. K. Synthesis, Spectroscopic Characterization and Thermal Studies of some Rare Earth Metal Complexes of Unsymmetrical Tetradentate Schiff Base Ligand. *Arabian Journal of Chemistry*, **2012a**, *5*(4), 501-507.
53. Ogawa, T.; Sinha, N.; Pfund, B.; Prescimone, A.; Wenger, O. S. Molecular Design Principles to Elongate the Metal-to-Ligand Charge Transfer Excited-State Lifetimes of Square-Planar Nickel (II) Complexes. *Journal of the American Chemical Society*, **2022**, *144*(48), 21948-21960.
54. Ikram, M.; Rehman, S.; Baker, R. J.; Rehman, H. U.; Khan, A.; Choudhary, M. I. Synthesis and Distinct Urease Enzyme Inhibitory Activities of Metal Complexes of Schiff-Base Ligands: Kinetic and Thermodynamic Parameters Evaluation from TG-DTA Analysis. *Thermochimica acta*. **2013**, 555, 72-80.
55. Nakatsukasa, T.; Matsuyanagi, K.; Matsuo, M.; Yabana, K. Time-Dependent Density-Functional Description of Nuclear Dynamics. *Rev Mod Phys*. **2016**, 88(4), 045004.
56. Parthasarathi, R.; Padmanabhan, J.; Subramanian, V.; Sarkar, U.; Maiti, B.; Chattaraj, P. Toxicity Analysis of Benzidine through Chemical Reactivity and Selectivity Profiles: A DFT Approach. *Int. Electron Jour. Mol*. **2003**, 2, 798–813.
57. Targema, M.; Obi-Egbedi, N. O.; Adeoye, M. D. Molecular Structure and Solvent Effects on the Dipole Moments and Polarizabilities of some Aniline Derivatives. *Comput. Theor.Chem*. **2013**, 1012, 47–53.
58. Iwanaga, T.; Kobayashi, D.; Hirayama, M.; Maeda, M.; Tamai, I. Involvement of Uric Acid Transporter in Increased Renal clearance of the Xanthine Oxidase Inhibitor Oxypurinol Induced by a Uricosuric Agent, Benzbromarone. *Drug Metabolism and Disposition*, **2005**, 33(12), 1791 – 1795.
59. Becker, M.A.; Schumacher, H. R.; Wortmann, R. L.; MacDonald, P. A.; Palo, W. A.; Eustace, D.; Vernillet, L.; Joseph-Ridge, N. Febuxostat, a Novel Nonpurine Selective Inhibitor of Xanthine Oxidase: A Twenty-Eight-Day, Multicenter, Phase II, Randomized, Dose-Response Clinical.
60. Abd El-halim, H. F.; Omar, M. M.; Mohamed, G. G. Synthesis, Structural, Thermal Studies and Biological Activity of a Tridentate Schiff Base Ligand and their Transition Metal Complexes. *Spectrochimica Acta Part A: Molecular and Biomolecular Spectroscopy*, **2011**, 78(1), 36-44.
61. Shiekh, R. A.; Said, M. A.; Malik, M. A.; Hashmi, A. A. Antimicrobial and Antioxidant Studies of Novel Mixed-Metal Complexes of Benzoyl-Aminoethanoic Acid-Nicotinamide: Microwave-Assisted Green Synthesis, Spectroscopic Characterization and Molecular Modeling. *Tropical Journal of*

Pharmaceutical Research, **2018**, 17(5), 865-874.

62. Ashrafuzzaman, M. D.; Camellia, F. K.; Mahmud, A. A.; Pramanik, M. D.; Nahar, K., Haque, M. Bioactive Mixed Ligand Metal Complexes of Cu (II), Ni (II), And Zn (II) Ions: Synthesis, Characterization, Antimicrobial and Antioxidant Properties. *Journal of the Chilean Chemical Society*, **2021**, 66(3), 5295-5299.

